Image-based metric heritage modeling in the near-infrared spectrum

Efstathios Adamopoulos (efstathios.adamopoulos@unito.it)
Universita degli Studi di Torino Dipartimento di Informatica https://orcid.org/0000-0003-4358-474X
Alessandro Bovero
Fondazione Centro Conservazione e Restauro dei Beni Culturali 'La Venaria Reale'
Fulvio Rinaudo
Politecnico di Torino Dipartimento di Architettura e Design

Research article

Keywords: Image-based modeling, Photogrammetry, Near-infrared imaging, Modified cameras, Heritage recording

Posted Date: March 28th, 2020

DOI: https://doi.org/10.21203/rs.3.rs-19268/v1

Version of Record: A version of this preprint was published at Heritage Science on June 5th, 2020. See the published version at https://doi.org/10.1186/s40494-020-00397-w.

Abstract

Digital photogrammetry and spectral imaging are widely used in heritage sciences, towards the comprehensive recording, understanding, and protection of historical artefacts and artworks. The availability of consumer-grade modified cameras for spectral acquisition, as an alternative to expensive multispectral sensors and multi-sensor apparatuses, along with semi-automatic software implementations of Structure-from-Motion (SfM) and Multiple-View-Stereo (MVS) algorithms, has made more feasible than ever the combination of those techniques. In the research presented here, the authors assess image-based modeling from near-infrared (NIR) imagery acquired with modified sensors, with applications on tangible heritage. Three-dimensional meshes, textured with the non-visible data, are produced and evaluated. Specifically, metric evaluations are conducted through extensive comparisons with models produced with high-resolution visible (VIS) spectrum image-based modeling, to check accuracy of results. Furthermore, the authors observe and discuss, when the implemented NIR modeling approach, enhances the preservation of surface detail on the reconstructed spectral models or counteracts certain problems arising from lighting conditions during VIS acquisition. Radiometric properties of the produced results are evaluated on the capacity to enhance observation towards the characterization of surface and under-surface state of preservation, and consequently, to support conservation interventions, in comparison to the respective results in visible spectrum.

Introduction

Multi-view image recording

In the course of the last decade, rapid advancements in passive sensors for reality capture, workflows for swift data acquisition, automatic or semi-automatic software implementing image-based reconstruction algorithmic approaches and computational systems for processing of large datasets have taken place. As a result, a profound expansion over the use of 3D image-based modeling technologies, over almost every aspect of archaeological science, has been observed.

Multi-view image recording [1, 2] has prevailed as a low-cost, efficient and easily implementable technique for cultural heritage documentation, interpretation, dissemination and protection [3–5]. Multi-view image approaches facilitate the digitization of tangible heritage with reduced needs for supervision and expertise. Concomitantly, they enable production of accurate and high-resolution results with images from relatively low-cost digital cameras. These approaches differ from traditional close-range photogrammetry, due to the capacity of effectively involving oblique imagery, and simultaneously estimating the internal and external orientation camera parameters, without the need for prior definition of control points of known coordinates on a reference system [6, 7]. However, their implementation is recommended during orientation for more accurate results and is mandatory for georeferencing. For applications that only require scaling in a local coordinate system a simple distance can enough for referencing. The processing pipeline starts with feature detection and description on every image of the dataset. Then follows a Structure-from-Motion (SfM) implementation to determine camera positions in 3D space and the coordinates of the scene, producing a sparse point cloud. Given the camera orientations, dense image matching algorithms enable further densification of the point cloud, as almost every pixel of the scene is reconstructed in 3D -a procedure typically named Multiple-View-Stereo (MVS) or dense stereo-matching. Later these dense point clouds can be transformed into textured models via surfacing algorithms and texture mapping.

Applications of terrestrial multi-view image-based modeling and texturing for large-scale heritage applications vary considerably. This technique has been implemented towards high resolution documentation and virtual restoration of small artefacts [8], damaged pottery [9], rock art [10], wall paintings [11] and decorative friezes [12], comprehensive investigations on pre-historic engravings [13], ancient Egyptian coffins [14] and ancient inscriptions [15], and evaluation of damage [16] and restoration works [17] on painted surfaces.

Near-infrared imaging and modeling

In the context of many heritage analyses, and especially for the study of polychromatic artworks or the investigation of surface or undersurface deterioration of historical artefacts, the use of visible-spectrum textures is often not adequate. Near-infrared imaging has often been explored towards this direction [18, 19], with sensors employing complementary metal-oxide-semiconductors (CMOS) based on InGaAs (indium gallium arsenide, 750–1700 nm) or PtSi (platinum silicide, 750–5000 nm) detectors, developed in the 1990s [20–22], and multispectral (up to 14 narrow spectral bands) single-point scanning systems, which significantly reduce the effects of optical and geometrical non-uniformities regarding multi-detectors arrays [23, 24].

Recently, the use of commercial digital cameras employing CCD (charge-coupled device) and CMOS sensors, modified for near-infrared or full spectrum acquisition (combined with external NIR filters) has been commonized in heritage science. They consist a lower cost, high-resolution alternative with spectral imaging capabilities, which retains user-friendly features and interfaces to a broad variety of photographic accessories and software [25–28].

The availability of high-resolution easily operated digital cameras for NIR acquisition, in combination with SfM/MVS image-based modeling techniques, has made feasible the 3D spectral modeling for heritage applications. Contemporary research which showed promising results [29–32] led us to the motivation for further experimentation.

Research aims

In this work, we are evaluating the use of imagery from consumer-grade digital reflex cameras modified for near-infrared imaging, in combination with image-based 3D reconstruction techniques, to produce high-fidelity models of tangible heritage assets textured with spectral information. To perform a thorough evaluation of this combined approach, we have acquired rigid image datasets for case studies of archaeological importance with varied dimensions and geometry, attempting to maintain constant most parameters of the acquisition for the visible and non-visible spectra involved. We produced 3D meshes utilizing software of different algorithmic implementations and compared the data produced by each method, in terms of surface deviation. Furthermore, we explored the usability of produced spectral textures. The principal aims of our research were to objectively quantify the quality of the 3D models produced by

this integrated spectral modeling method, to assess applicability for different heritage case studies, to understand how this method can potentially enhance the preservation of surface detail on the reconstructed 3D digital models, and finally, to discuss the radiometric capacity of the fabricated near-infrared textures, for augmenting observations towards the characterization of the state-of-preservation and subsequently, to support conservation planning.

Materials And Methods

Case studies

To evaluate the presented approach, combining multi-view photogrammetric modeling and near-infrared spectral imaging from modified camera sensors, four heritage artwork case studies of dissimilar characteristics were involved. The first one was a 17th century marble statue (approx. height 1.75 m) from the Fountain of Hercules at the Reggia di Venaria Reale near Turin. The Palace of Venaria was one of the Residences of the Royal House of Savoy, included in the UNESCO World Heritage List in 1997. The statue is owned by Musei Reali Torino.

The second case study was a 18th century Chinese Coromandel screen folding panel from Castello di Grinzane Cavour (Santena, Province of Turin, Piedmont). The castle's history starts around 1350, it was owned by several lords, the most famous of which was, in the mid-19th century, Camillo Benso, Conte di Cavour, who resided there starting from 1830 and restored the construction. It was inscribed on UNESCO World Heritage List in 2014. The object is owned by the City of Turin – Cavour Foundation.

The third case study was an 18th century wooden furniture part painted with flowers (2.39 × 0.81 m^2), from the Sala dell'Alcova in Palazzo Chiablese. The Palazzo Chiablese is a wing of the Royal Palace of Turin. It was the residence of the Duke of Chablais first and then of Carlo Felice, King of Sardinia, and Ferdinando, Duke of Genoa. The object is owned by the Italian Ministry of Cultural Heritage and Activities.

The fourth, and last, case study was a small 19th century religious plaster sculpture of Christ crucified (31 cmx22 cm) from Castello di Casotto (Garessio, Province of Cuneo, Piedmont) owned by the Region of Piedmont. The Casotto Castle was originally a Carthusian monastery, later acquired by the Savoy and transformed into a castle and hunting lodge by Carlo Alberto.

Instrumentation, software and tools

NIR images were collected using a Nikon D810 professional camera modified for near-infrared acquisition by MaxMax LDP and a low-cost Canon EOS Rebel SL1 camera modified for full-spectrum acquisition by LifePixel. The D810 is a Digital Single-Lens Reflex (DSLR) camera that employs a full-frame CMOS sensor (35.9 × 24 mm^2, 4.88 µm pixel size), with a maximum resolution of 36.3 effective Megapixels. The Rebel SL1 is a DSLR camera that employs an APS-C CMOS sensor (22.3 × 14.9 mm^2, 4.38 µm pixel size), with a maximum resolution of 18.0 effective Megapixels. For the NIR acquisition with the Rebel SL1 an external near-infrared pass (700–1400 nm) filter was utilized. VIS images were captured using a Canon EOS 1200D compact DSLR that employs an APS-C CMOS sensor (22.3 × 14.9 mm2, 4.40 µm pixel size), with a maximum resolution of 18.0 effective Megapixels. Also, the modified Canon EOS Rebel SL1, described above, was additionally used in combination with an external visible pass filter. In order to avoid camera micro-shake effects and to produce better quality photos, the cameras were mounted on a tripod. For all photo-editing operations, we used Adobe Lightroom Classic.

Multi-view image-based reconstruction was conducted with Agisoft Metashape Professional 1.5.1 (AMP) for the first case study, and additionally with 3DFlow Zephyr Aerial 4.519 (FZA) for the rest of the case studies, in order to also compare the performance of different algorithmic implementations with NIR imagery. Both commercial software are SfM/MVS approach based. Agisoft Metashape Professional employs SIFT-like detection and description, then calculates approximate camera location and used Global bundle-adjustment to refine them, a type of MVS disparity calculation for dense reconstruction and Screened Poisson surface reconstruction. 3DFlow Zephyr Aerial employs a modified Difference-of-Gaussian (DoG) detector, a combination of Approximate Nearest Neighbor Searching, M-estimator Sample Consensus and Geometric Robust Information Criterion for matching, then hierarchical SfM and Incremental adjustment, dense MVS reconstruction with fast visibility integration, tight disparity bounding and finally meshing with an edge-preserving algorithmic approach was selected to differentiate from Agisoft Metashape Professional. All processing were performed with the same computer. Parameters were selected to minimize surface noise and to optimize the final textured results, but at the same time we attempted to maintain as similar parameter values as possible between software and spectra, to ascertain the metrological validity of the conducted research.

Data acquisition

For the first two case studies lighting conditions were not optimal to acquire photogrammetric datasets. The marble statue was illuminated ununiformly by various spotlights and it was decided not to use flash as it was resulting in more radiometric contrasts instead of reducing them. The Coromandel lacquerware was also under ununiform lighting, with glaring effect visible on optical photos at the upper part, and flash could not be used, because of the highly reflective nature of the lacquer. For the rest of the case studies we were able to appropriately utilize flash, thus eliminating shadows, to acquire imagery datasets with as homogeneous radiometrical characteristics as possible. An x•rite ColorChecker® Classic with 24 colors was used for color balancing, utilizing middle gray for the visible-spectrum datasets and foliage green for the near-infrared color-balancing. Scaling was performed with an invar scale bar of 1.000165 m (± 15 nm), barring for the small plaster sculpture, where we used as reference the dimensions of the wooden cross. Additionally, small targets were placed on the base and body of the marble statue to facilitate further metric comparisons.

Dense acquisition of images was planned in such a manner as to acquire rigid datasets, with large overlaps (> 80%) from a very close range. Furthermore, it was attempted to maintain capturing conditions (internal, external orientation parameters and ground sampling distances) constant between VIS and NIR spectra, also taking into consideration the different sensors employed and the surrounding conditions, to obtain comparable results. Very low ISO values were used to prevent sensor luminance noise, simultaneously maintaining exposure under the clipping limit value. All images were acquired in RAW format. Acquisition conditions are summarized in Table 1.

Table 1
Characteristics of acquired image datasets.

Case study	Camera model	MP	f	Pixel size	Distance	GSD [mm]	Spectrum	No. images	f-stop	Exposure	ISO
1	EOS 1200D	18.0	18.0 mm	4.40 μm	0.98 m	0.21 mm	VIS	180	f/11	½ s	200
	D810	36.3	24.0 mm	4.88 μm	1.24 m	0.22 mm	NIR	180	f/11	5 s	200
2	REBEL-SL1	18.0	18.0 mm	4.38 μm	2.57 m	0.56 mm	VIS	22	f/16	1 s	100
	REBEL-SL1	18.0	18.0 mm	4.38 μm	2.68 m	0.59 mm	NIR	22	f/16	1 s	100
3	REBEL-SL1	18.0	18.0 mm	4.38 μm	72 cm	0.16 mm	VIS	40	f/16	2.5 s	100
	REBEL-SL1	18.0	18.0 mm	4.38 μm	73 cm	0.16 mm	NIR	40	f/16	2.5 s	100
4	REBEL-SL1	18.0	55.0 mm	4.38 μm	26 cm	0.02 mm	VIS	60	f/16	1/15 s	100
	REBEL-SL1	18.0	55.0 mm	4.38 μm	26 cm	0.02 mm	NIR	60	f/16	1/15 s	100

Data processing

Image-based reconstruction from visible and near-infrared imagery followed a semi-automatic SfM/MVS workflow, standard for large-scale archaeological photogrammetric applications [33, 34], very similar on both employed software, despite considerable differences on the algorithmic implementations. It should be underlined that chosen processing parameters remained unchanged (when applicable) between software and spectra.

Before processing, raw images were pre-processed to soften the highlights and the shadows up to the level that the features useful for image-based modeling would not be affected. In addition to that, the implemented images were masked accordingly, to exclude the unwanted areas of each scene, and, in the last case study, out-of-focus (blurry) areas on the plaster sculpture, to increase the quality of imagery, thus reducing noise both levels and processing times. Between each stage of the reconstruction, thorough visual checks were performed to determine quality, and denoising procedures were subsequently followed, in an identical manner for all the produced meshes, to not reduce comparability of results.

The 3D models were semi-automatically generated in a four-step process. The first step included a sparse reconstruction of each scene, with simultaneous approximate calculation of cameras' relative orientation at the moment of image acquisition, and autocalibration, with SfM approaches. For this step, the selected accuracy and density parameters were the highest available in both software. The sparse point clouds were cleaned according to reprojection errors, and local cluster distances with statistical filtering. During the second step, the results were densified by employing MVS stereo-matching algorithms. The third step consisted of meshing the dense 3D point clouds into triangular surfaces (3D Delaunay algorithm). The produced meshes were then cleaned from small unconnected components and spikes. The final step referred to the application of texture mapping to obtain single-file high-resolution textures from the original photographs. Given the high quality of the original imagery we limited color balancing and blending between images to reduce the possibility of radiometric errors. Into choosing the resolution of textures we considered sampling distances to be at least two or three times higher than the original pixel sizes.

Results And Discussion

With the intention of evaluating the photogrammetric results we recorded in detail the processing times, reconstruction errors and volumes of the results, catalogued in Table 2. Detailed geometric comparisons were performed, to assess surface deviations among visible and near-infrared models, as well as amongst software, by computing distances between the vertices of the final meshes. This task was performed in the open source software CloudCompare with the Cloud-to-Cloud Hausdorff distances tool.

Table 2
Image-based reconstruction processing results.

Case study	1		2				3				4		
Spectrum	VIS	NIR	VIS	NIR	VIS	NIR	VIS	NIR	VIS	NIR	VIS	NIR	VIS
Software	AMP	AMP	AMP	AMP	FZA	FZA	AMP	AMP	FZA	FZA	AMP	AMP	FZA
Sparse cloud													
Images Aligned	180	180	22	22	22	22	40	40	40	40	60	60	60
Matching time [mm:ss]	05:16	14:46	00:34	00:29	04:02	04:02	01:16	01:07	07:08	07:14	01:55	01:23	43:56
Alignment time [mm:ss]	05:33	07:33	00:09	00:15	01:08	01:30	00:15	00:17	01:19	00:58	01:19	00:47	04:31
Tie points [1, 000]	454	151	94	87	28	28	81	71	43	44	420	236	132
Projections [1, 000]	1,434	467	364	353	341	253	212	208	217	215	1,270	643	803
Reprojection error [pixels]	0.65	0.72	0.58	0.69	0.82	0.83	0.90	0.93	1.08	1.10	0.35	0.48	0.47
Dense cloud													
Processing time [mm:ss]	1:43:36	1:57:41	08:17	08:52	16:53	18:00	07:07	07:48	37:19	29:27	14:27	15:15	42:16
Point count	14,676	15,122	5,879	5,394	1,748	1,840	25,554	26,542	6,527	4,276	10,005	10,082	3,959
Mesh													
Processing time [mm:ss]	08:35	15:14	01:41	01:22	03:35	03:35	13:40	14:33	08:49	09:02	02:58	02:58	03:34
Triangle count [1, 000]	25,000	25,000	10,000	10,000	1,500	1,208	10,000	10,000	6,092	5,754	12,084	12,036	5,410
Vertices count [1, 000]	12,500	12,474	5,089	5,010	785	666	4,948	4,978	3,071	2,946	6,075	6,079	3,039
Texture													
Processing time [mm:ss]	44:49	38:00	1:12:45	03:15	02:26	02:06	03:04	02:58	07:07	06:57	29:46	22:23	09:50
Overall													
Total time [h:mm:ss]	2:47:49	3:13:14	1:23:26	0:14:13	0:28:04	0:29:13	0:25:22	0:26:43	1:01:42	0:53:38	0:50:25	0:42:46	1:44:07

In the case study of the marble statue (Fig. 1), both spectral scenarios resulted in full digital reconstructions of the scene. Near-infrared image-based modelin produced sparser initial results than the visible spectrum modeling, however dense results were of the same volumes and were produced in comparable times NIR mesh contained a very low level of surface noise, especially in areas with less overlapping images, although the surface details had been equally preserv terms of geometric differences, the two models produced with Metashape Pro fluctuated by 0.7 mm ± 0.6 mm (Fig. 2), meaning a differentiation of less than times the GSD (1 RMS) or less than 2.5‰ of the smallest dimension of the object. Thus, considering the evaluated precision of the method, the models can b considered metrically identical and could be interchangeable for geometric recording and visualization on an up to 1:5 scale -very common for applications o mapping. Texturing results were of the same quality. As visible, shadows could not be effectively eliminated on either scenario.

Observations on the 3D texture results for the marble statue showed that generally, higher near-infrared intensities correspond to healthier areas of the marble's surface, whereas lower intensities correspond to more deteriorated areas (Fig. 3). Thus, the NIR three-dimensional textured mesh could be used to roughly visualize in 3D the levels of decay on the statue. Undeniably, a complete elimination of shadows would help optimize these results. We should further underline, that under no circumstance could this visualization substitute the detailed chemical characterizations. Although, for small, homogeneously shadowed areas of the same material, it can provide a rapid approximation of the state-of-preservation and quantification of decay.

Regarding the case study of the lacquered screen panel, the mesh produced from NIR imagery by Metashape Pro was the only complete one and had the higher quality of surface detail. Metashape Pro produced about three-times denser results than Zephyr Aerial, but the imaging spectrum did not seem to have significant effect on the density. However, the geometry of the 3D VIS models was problematic, highlighting the consequences of the glaring effect during visible spectrum data capturing (Fig. 4). Zephyr Aerial models were noisier than those produced by Metashape Pro. For Zephyr Aerial, processing times were

comparable among separate spectra, despite the substantial difference in Metashape Pro, caused by the very fragmented triangular 3D mesh which slowed down significantly the texturing algorithm. Distances between VIS and NIR geometries recorded with Metashape Pro were 1.0 mm ± 0.8 mm, meaning a differentiation of less than three-times the GSD (1 RMS), again, metrically very similar, considering the precision of the method. Still, distances computed for Zephyr Aerial were 2.2 mm ± 1.6 mm, which should be considered significant. Additionally, differences between the VIS models produced with different software ranged between 2-2.5 mm, same as for the NIR models. As observed, the differences calculated between the 'perforated' Metashape Pro VIS model and the respective NIR model, corresponded roughly to deficiencies and noise of the digitization in visible spectrum (Fig. 5).

High-resolution modeling and texturing with near-infrared imagery, did not only produce better topological results for the case study of the Chinese lacquerware, but also enabled the identification of previous conservation interventions that are not recognizable on the visible textures and cannot be easily observed otherwise (Fig. 6).

For the case study of the wooden furniture part all scenarios produced high-resolution results, with reconstruction errors of the same grade of magnitude (0.35–0.50 pixels). Although, final point clouds for Zephyr Aerial were approximately five times sparser and were produced in double the processing time. Distances between VIS and NIR geometries recorded with Metashape Pro were 2.2 mm ± 1.4 mm, and 2.4 mm ± 2.0 mm with Zephyr Aerial. These differences can be interpreted as significant inaccuracies, regarding to the size of the pixel on the object (0.02 mm), but if we consider the 2 ÷ 4 mm differences between VIS models of the two software as precision of the methodology, then they can be accepted (Fig. 7). A percentage of this problem though, can be attributed to the flat almost two-dimensional geometry of the object that doesn't favor the reconstruction. In addition to that, both 3D models from Zephyr Aerial included medium levels of noise. On the contrary, the respective 3D models from Metashape Pro had a very smooth surface while preserving most of the detail (Fig. 8).

The detail on acquired texturing results both for visible and near infrared was adequate for conservation-oriented observations. With the near-infrared textures we were able to successfully locate and measure cracks, paint defects and retouchments (Fig. 9.)

Regarding the last case study, that of the plaster sculpture of Christ crucified, all processing scenarios resulted in very high detail and high texture-quality models (Fig. 10). Only the triangular 3D mesh produced with the NIR imagery from Zephyr Aerial, contained a low magnitude of noise. Unlike to the other case studies, Zephyr Aerial produced sparser results than Metashape Pro both for the NIR and the VIS images. The initial reconstructions of the object were sparser in near-infrared but, dense reconstruction results were of very similar volume for VIS and NIR imagery in both software. Zephyr Aerial required longer processing times. The variation between VIS and NIR vertices ranged below 0.15 mm (0.08 mm ± 0.07 mm) for both software, a very accurate result considering the GSD of original photos, the precision of the method, the type of sensor, and the distances between the visible models, which had a 0.11 mm ± 0.14 mm (Fig. 11).

The very-high-resolution NIR textures made feasible the identification of deterioration and were further exploited to roughly map the different levels of state of preservation (Fig. 12). This detailed mapping could assist the precise work required by conservators on such very-large scale restoration applications.

Conclusions

In this work, we constructed detailed models of historical artwork with high-resolution near-infrared textures, combining multi-view image 3D recording and near-infrared images captured with modified DSLR cameras, thus proving the feasibility of this integrated technique. Apart from the obvious advantage of reduced cost, comparing to previously applied near-infrared three-dimensional acquisition methods, we also observed an increased versatility and convenience of implementation. We used two commercial software to compare the behavior of different Structure-from-Motion, Multiple-View-Stereo, and Meshing algorithmic implementations in near-infrared. Metashape Pro generally provided more complete and less noisy meshes than Zephyr Aerial, with higher density and slightly smaller statistical reconstruction errors. Furthermore, we constructed as reference, detailed models of the same heritage case studies from visible imagery, acquired under the same conditions, and processed with similar parameters, to ensure comparability. We observed that the initial reconstruction results from all case studies were sparser in near-infrared, with slightly heightened reconstruction errors, but the dense results were of very similar volume and produced on comparable times. For the case study of a Chinese screen panel, which was from highly reflective material, digitization from near-infrared imagery even improved the reconstruction results, compensating for the glaring effects under visible light. Metric checks for all case studies proved that the combined 3D spectral technique is also very accurate comparing to visible 3D image-based modeling, by taking into consideration sensors, lenses, capturing distances, and the precision of SfM/MVS based approaches. The high-resolution infrared textures improved the visibility of deterioration on the sculptures, potentially providing a valuable low-cost tool for three-dimensional decay mapping, if certain light conditions are met during the data acquisition. In addition, they assisted identification of defects and previous restoration works on the lacquerware and painted surfaces case studies, thus ascertaining the significance of the discussed approach, towards heritage restoration and protection.

Abbreviations

2D: Two-Dimensional; 3D: Three-Dimensional; AMP: Agisoft Metashape Professional; CCD: Charge-Coupled Device; CMOS: Complementary Metal-Oxide-Semiconductors; DSLR: Digital Single-Lens Reflex camera; FZA: 3DFlow Zephyr Aerial; GSD: Ground Sampling Distance; MVS: Multiple-View-Stereo; NIR: Near-InfraRed; RMS: Round Square Mean; RMSE: Round Square Mean Error; SfM: Structure-from-Motion; VIS: VISible

Declarations

Availability of data and materials

The datasets used and/or analyzed during the current study are available from the corresponding author on reasonable request.

Competing interests

The authors declare that they have no competing interests.

Funding

This project has received funding from the European Union's Framework Programme for Research and Innovation Horizon 2020 (2014 – 2020) under the Marie-Skłodowska Curie Grant Agreement No. 754511 and from the Compagnia di San Paolo, Turin.

Authors' contributions

Efstathios Adamopoulos: Conceptualization, Methodology, Validation, Formal analysis, Investigation, Writing - Original Draft, Visualization. Alessandro Bovero: Resources, Writing – Review & Editing, Supervision. Fulvio Rinaudo: Resources, Writing – Review & Editing, Supervision, Project administration, Funding acquisition

Acknowledgements

The authors would like to acknowledge Musei Reali Torino for the courteous concession of permission to publish the results about the statue from the Fountain of Hercules, Città di Torino - Fondazione Cavour for the courteous concession of permission to publish the results about the four-panel Coromandel Screen, Ministero per i Beni e le Attività Culturali for the courteous concession of permission to publish the results about the wooden furniture part, and Ragione Piemone for the courteous concession of permission to publish results about the sculpture of Christ crucified. The authors would also like to acknowledge the contribution of Marianna Ferrero and Dr. Stefania De Blasi, heads of Laboratories and Documentation, and Programming and Communications respectively, at the Department of Programming and Development at Fondazione Centro Conservazione e Restauro dei Beni Culturali 'La Venaria Reale' in making possible the publishing of results produced at the scientific labs of the aforementioned conservation and restoration center. Furthermore, the authors would like to acknowledge Marie Claire Canepa coordinator of the Lab for Mural Paintings, Stonework And Architectural Surfaces at Fondazione Centro Conservazione e Restauro dei Beni Culturali 'La Venaria Reale' for facilitating the data acquisition for the statue case study.

References

1. Koutsoudis A, Vidmar B, Ioannakis G, Arnaoutoglou F, Pavlidis G, Chamzas C. Multi-image 3D reconstruction data evaluation. Journal of Cultural Heritage. 2014;15(1):73-79. doi:10.1016/j.culher.2012.12.003
2. Georgopoulos A, Stathopoulou EK. Data Acquisition for 3D Geometric Recording: State of the Art and Recent Innovations. In: Vincent ML, López-Menchero Bendicho VM, Ioannides M, Levy TE, eds. Heritage and Archaeology in the DigitalAge. Cham: Springer International Publishing; 2017:1-26. doi:10.1007/978-3-319-65370-9_1
3. McCarthy J. Multi-image photogrammetry as a practical tool for cultural heritage survey and community engagement. Journal of Archaeological Science. 2014;43:175-185. doi:10.1016/j.jas.2014.01.010
4. Cabrelles M, Blanco-Pons S, Carrión-Ruiz B, Lerma JL. From Multispectral 3D Recording and Documentation to Development of Mobile Apps for Dissemination of Cultural Heritage. In: Levy TE, Jones IWN, eds. Cyber-Archaeology and Grand Narratives. Cham: Springer International Publishing; 2018:67-90. doi:10.1007/978-3-319-65693-9_5
5. Georgopoulos A. Contemporary Digital Technologies at the Service of Cultural Heritage. In: Chanda B, Chaudhuri S, Chaudhury S, eds. Heritage Preservation. Singapore: Springer Singapore; 2018:1-20. doi:10.1007/978-981-10-7221-5_1
6. Westoby MJ, Brasington J, Glasser NF, Hambrey MJ, Reynolds JM. 'Structure-from-Motion' photogrammetry: A low-cost, effective tool for geoscience applications. Geomorphology. 2012;179:300-314. doi:10.1016/j.geomorph.2012.08.021
7. Fonstad MA, Dietrich JT, Courville BC, Jensen JL, Carbonneau PE. Topographic structure from motion: a new development in photogrammetric measurement. Earth Surf Process Landforms. 2013;38(4):421-430. doi:10.1002/esp.3366
8. Kai-Browne A, Kohlmeyer K, Gonnella J, et al. 3D Acquisition, Processing and Visualization of Archaeological Artifacts. In: Ioannides M, Fink E, Moropoulou A, et al., eds. Digital Heritage. Progress in Cultural Heritage: Documentation, Preservation, and Protection. Vol 10058. Cham: Springer International Publishing; 2016:397-408. doi:10.1007/978-3-319-48496-9_32
9. Rodríguez González E, Pastor SC, Casals JR. Lost colours: Photogrammetry, image analysis using the DStretch plugin, and 3-D modelling of post-firing painted pottery from the south west Iberian Peninsula. Digital Applications in Archaeology and Cultural Heritage. 2019;13:e00093. doi:10.1016/j.daach.2019.e00093
10. Bea M, Angás J. Geometric documentation and virtual restoration of the rock art removed in Aragón (Spain). Journal of Archaeological Science: Reports. 2017;11:159-168. doi:10.1016/j.jasrep.2016.11.025
11. Higuchi R, Sugawara H, Gülyaz ME. PHOTOGRAMMETRY USING VIRTUAL RESTORATION OF WALL-PAINTINGS OF THE ROCK-HEWN CHURCHES IN THE GÖREME VALLEY, CAPPADOCIA AND ITS VALUE FOR THE MUSEUM'S CONTENTS. ISPRS Ann Photogramm Remote Sens Spatial Inf Sci. 2019;IV-2/W6:83-89. doi:10.5194/isprs-annals-IV-2-W6-83-2019
12. Tucci G, Bonora V, Conti A, Fiorini L. High-quality 3D models and their use in a cultural heritage conservation project. Int Arch Photogramm Remote Sens Spatial Inf Sci. 2017;XLII-2/W5:687-693. doi:10.5194/isprs-archives-XLII-2-W5-687-2017

13. Porter ST, Huber N, Hoyer C, Floss H. Portable and low-cost solutions to the imaging of Paleolithic art objects: A comparison of photogrammetry and reflectance transformation imaging. Journal of Archaeological Science: Reports. 2016;10:859-863. doi:10.1016/j.jasrep.2016.07.013
14. Mandelli A, Perfetti L, Fiorillo F, Fassi F, Rossi C, Greco C. The Digitalization of Ancient Egyptian Coffins: A Discussion over Different Techniques for Recording Fine Details. Int Arch Photogramm Remote Sens Spatial Inf Sci. 2019;XLII-2/W15:743-750. doi:10.5194/isprs-archives-XLII-2-W15-743-2019
15. Andreu J, Serrano P. Contributions of the digital photogrammetry and 3D modelling of Roman inscriptions to the reading of damaged tituli: An example from the Hispania Tarraconensis (Castiliscar, Saragossa). Digital Applications in Archaeology and Cultural Heritage. 2019;12:e00091. doi:10.1016/j.daach.2019.e00091
16. Angheluță LM, Rădvan R. Macro Photogrammetry for the Damage Assessment of Artwork Painted Surfaces. Int Arch Photogramm Remote Sens Spatial Inf Sci. 2019;XLII-2/W15:101-107. doi:10.5194/isprs-archives-XLII-2-W15-101-2019
17. Abate D. Documentation of paintings restoration through photogrammetry and change detection algorithms. Herit Sci. 2019;7(1):13. doi:10.1186/s40494-019-0257-y
18. Fischer C, Kakoulli I. Multispectral and hyperspectral imaging technologies in conservation: current research and potential applications. Studies in Conservation. 2006;51(sup1):3-16. doi:10.1179/sic.2006.51.Supplement-1.3
19. Liang H. Advances in multispectral and hyperspectral imaging for archaeology and art conservation. Appl Phys A. 2012;106(2):309-323. doi:10.1007/s00339-011-6689-1
20. Delaney JK, Zeibel JG, Thoury M, et al. Visible and Infrared Imaging Spectroscopy of Picasso's Harlequin Musician: Mapping and Identification of Artist Materials in Situ. Appl Spectrosc. 2010;64(6):584-594. doi:10.1366/000370210791414443
21. Bendada A, Sfarra S, Ibarra−Castanedo C, et al. Subsurface imaging for panel paintings inspection: A comparative study of the ultraviolet, the visible, the infrared and the terahertz spectra. Opto-Electronics Review. 2015;23(1). doi:10.1515/oere-2015-0013
22. Miguel C, Bottura S, Ferreira T, Conde AF, Barrocas-Dias C, Candeias A. Unveiling the underprintings of a late-fifteenth-early-sixteenth century illuminated French incunabulum by infrared reflectography. Journal of Cultural Heritage. 2019;40:34-42. doi:10.1016/j.culher.2019.05.014
23. Obrutsky A, Acosta D. Reflectography, a NDT method for images diagnosis. In: Proceedings 16th WCNDT - World Conference on NDT, Montreal, Aug 2004.
24. Daffara C, Pampaloni E, Pezzati L, Barucci M, Fontana R. Scanning Multispectral IR Reflectography SMIRR: An Advanced Tool for Art Diagnostics. Acc Chem Res. 2010;43(6):847-856. doi:10.1021/ar900268t
25. Cavaleri T, Buscaglia P, Lo Giudice A, et al. Multi and Hyperspectral Imaging and 3D Techniques for Understanding Egyptian Coffins. In: Strudwick H, Dawson J, eds. Ancient Egyptian Coffins: Past – Present – Future. Barnsley: Oxbow Books; 2019:43-51. 10.2307/j.ctvh9w0cw.
26. Pronti L, Romani M, Verona-Rinati G, et al. Post-Processing of VIS, NIR, and SWIR Multispectral Images of Paintings. New Discovery on the The Drunkenness of Noah, Painted by Andrea Sacchi, Stored at Palazzo Chigi (Ariccia, Rome). Heritage. 2019;2(3):2275-2286. doi:10.3390/heritage2030139
27. Triolo PAM, Spingardi M, Costa GA, Locardi F. Practical application of visible-induced luminescence and use of parasitic IR reflectance as relative spatial reference in Egyptian artifacts. Archaeol Anthropol Sci. 2019;11(9):5001-5008. doi:10.1007/s12520-019-00848-x
28. Willard C, Gibson AP, Wade N. High-resolution visible and infrared imaging for large paintings: a case study of Israel in Egypt by Poynter. In: Targowski P, Groves R, Liang H, eds. Optics for Arts, Architecture, and Archaeology VII. Munich, Germany: SPIE; 2019:50. doi:10.1117/12.2525714
29. Grifoni E, Legnaioli S, Nieri P, et al. Construction and comparison of 3D multi-source multi-band models for cultural heritage applications. Journal of Cultural Heritage. 2018;34:261-267. doi:10.1016/j.culher.2018.04.014
30. Webb EK, Robson S, MacDonald L, Garside D, Evans R. Spectral and 3D cultural heritage documentation using a modified camera. Int Arch Photogramm Remote Sens Spatial Inf Sci. 2018;XLII-2:1183-1190. doi:10.5194/isprs-archives-XLII-2-1183-2018
31. Adamopoulos E, Rinaudo F, Bovero A. First assessments on heritage science oriented image-based modeling using low-cost modified and mobile cameras. Int Arch Photogramm Remote Sens Spatial Inf Sci. 2019;XLII-2/W17:23-30. doi:10.5194/isprs-archives-XLII-2-W17-23-2019
32. Mathys A, Jadinon R, Hallot P. Exploiting 3D multispectral texture for a better feature identification for cultural heritage. ISPRS Ann Photogramm Remote Sens Spatial Inf Sci. 2019;IV-2/W6:91-97. doi:10.5194/isprs-annals-IV-2-W6-91-2019
33. Alsadik B, Gerke M, Vosselman G, Daham A, Jasim L. Minimal Camera Networks for 3D Image Based Modeling of Cultural Heritage Objects. Sensors. 2014;14(4):5785-5804. doi:10.3390/s140405785
34. De Reu J, Plets G, Verhoeven G, et al. Towards a three-dimensional cost-effective registration of the archaeological heritage. Journal of Archaeological Science. 2013;40(2):1108-1121. doi:10.1016/j.jas.2012.08.040

Figures

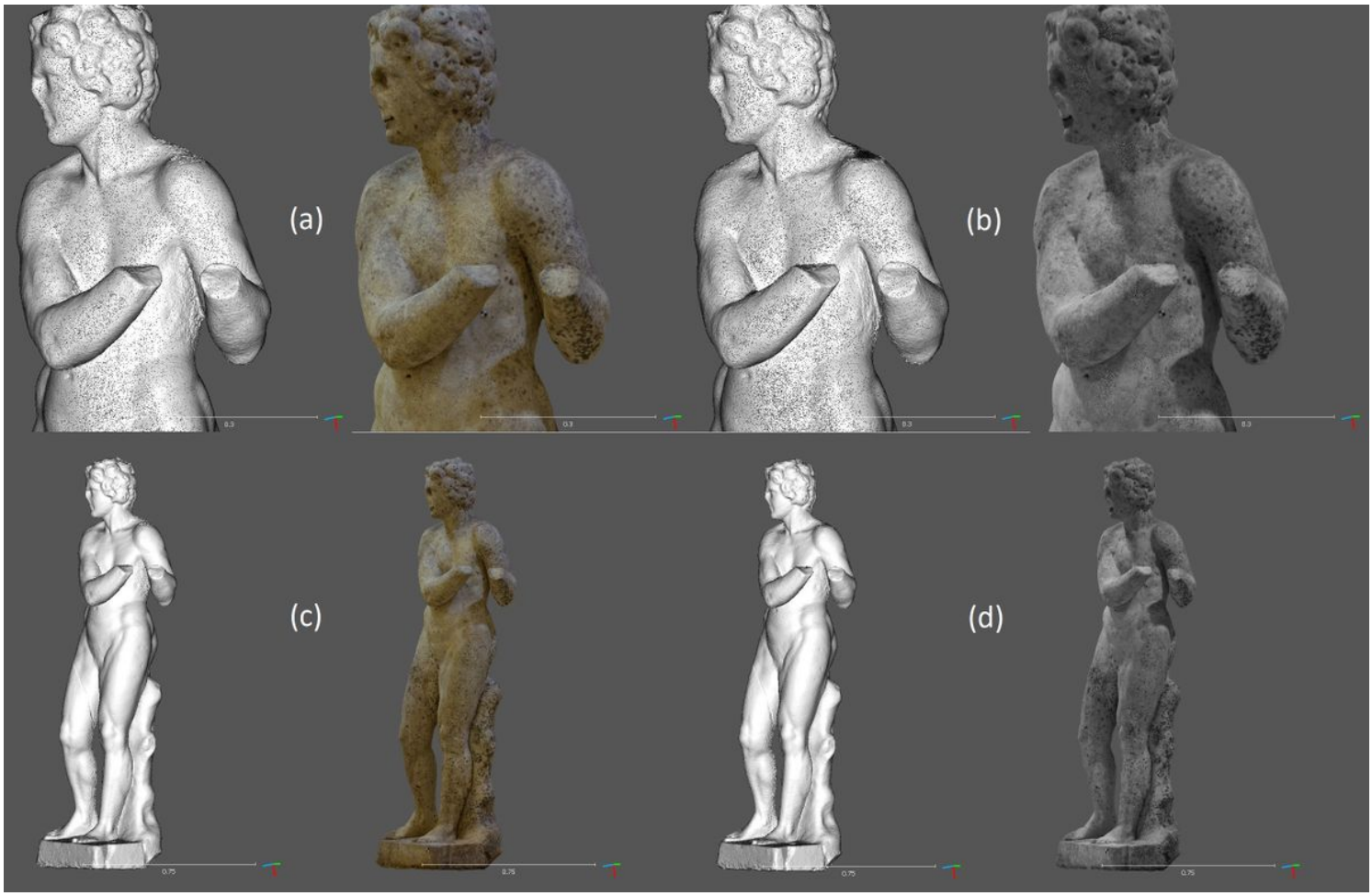

Figure 1

Marble statue, dense image-based reconstruction results (left untextured, right textured) a visible spectrum point cloud; b near-infrared spectrum point cloud; c visible spectrum mesh; d near-infrared spectrum mesh

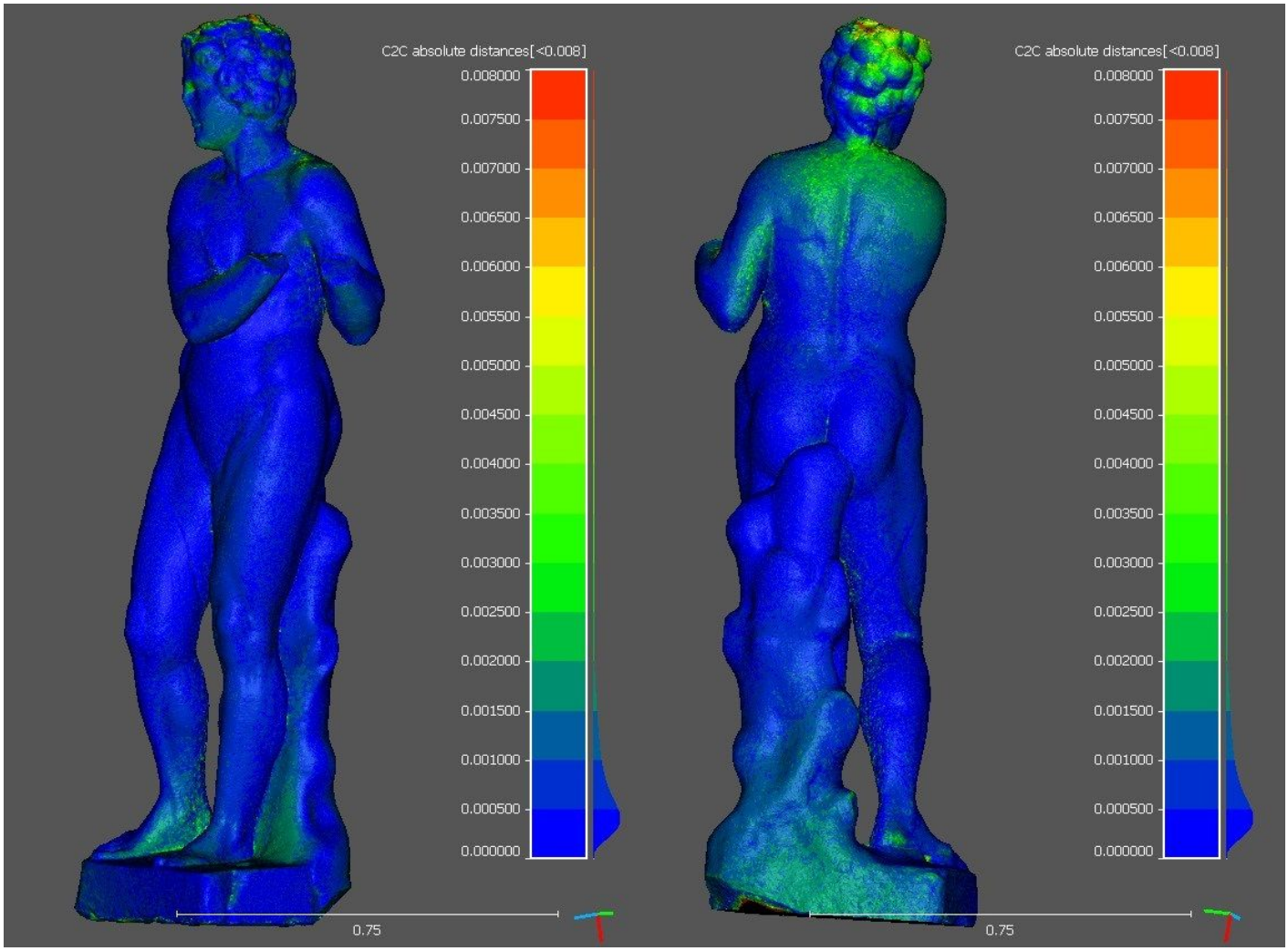

Figure 2

Marble statue, geometric differences between visible and near-infrared spectra models (Hausdorff distances shown on a scale up to 8 mm, with 0.5 mm scalar field intervals)

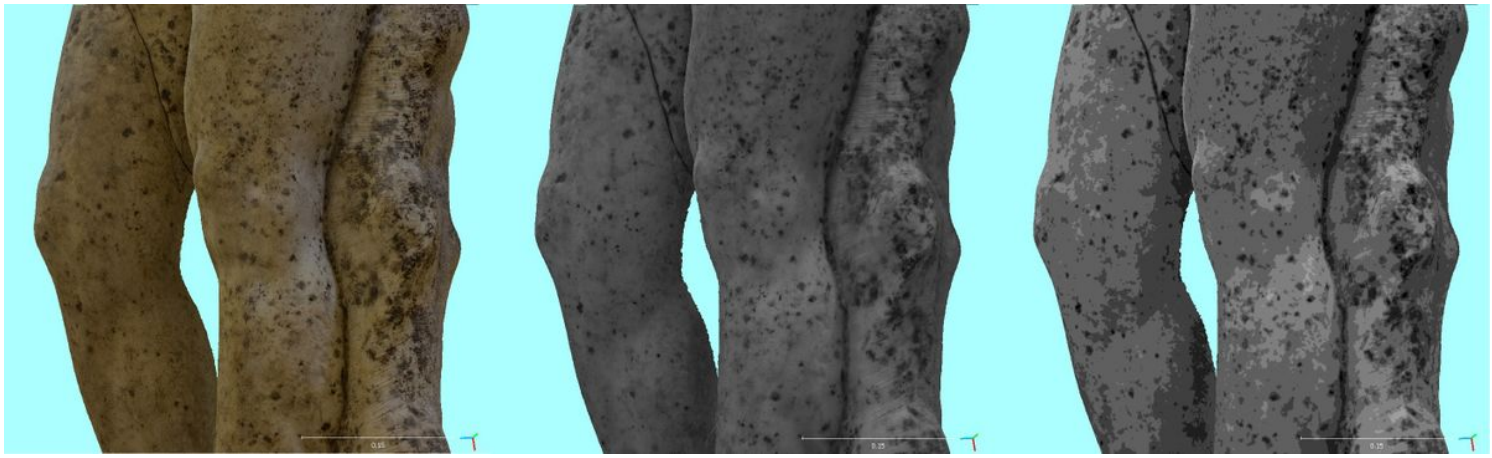

Figure 3

Marble statue, close-up comparison between visible (left), near-infrared (center) textures and 8-group classification mapping of near-infrared intensities (right)

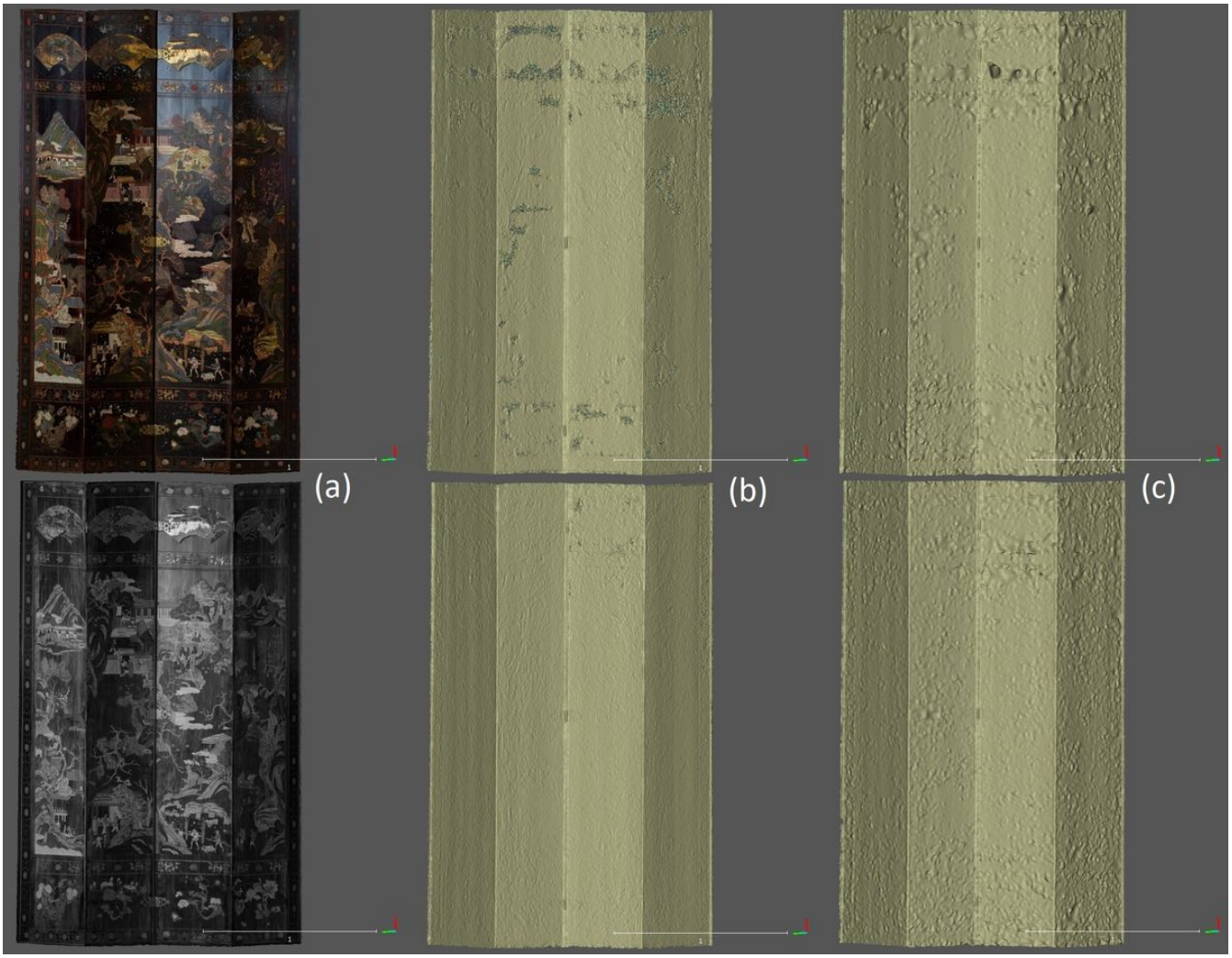

Figure 4

Screen panel, dense image-based reconstruction results (top visible spectrum, bottom near-infrared spectrum), a AMP textured mesh; b AMP untextured mesh; c FZA untextured mesh

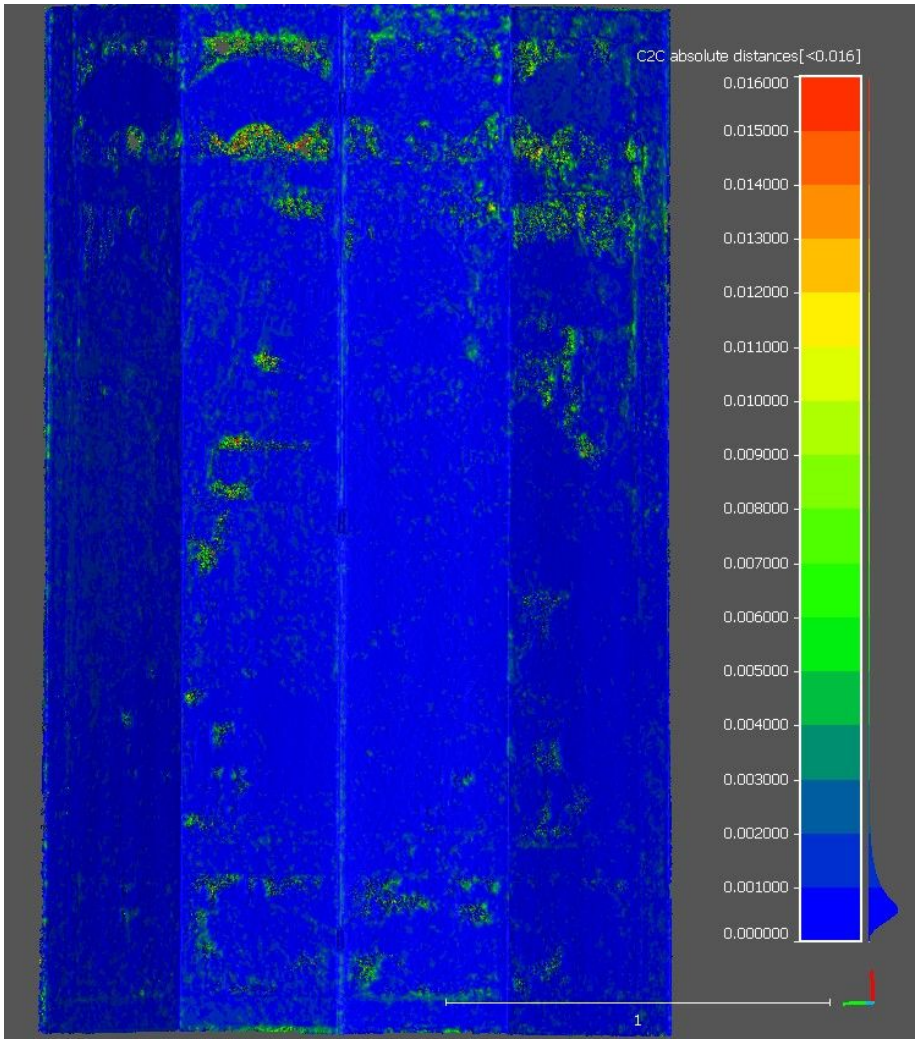

Figure 5

Screen panel, geometric differences between visible and near-infrared spectra AMP models (Hausdorff distances shown on a scale up to 16 mm, with 1 mm scalar field intervals)

Figure 6

Screen panel (detail), near-infrared model where previous interventions can be observed

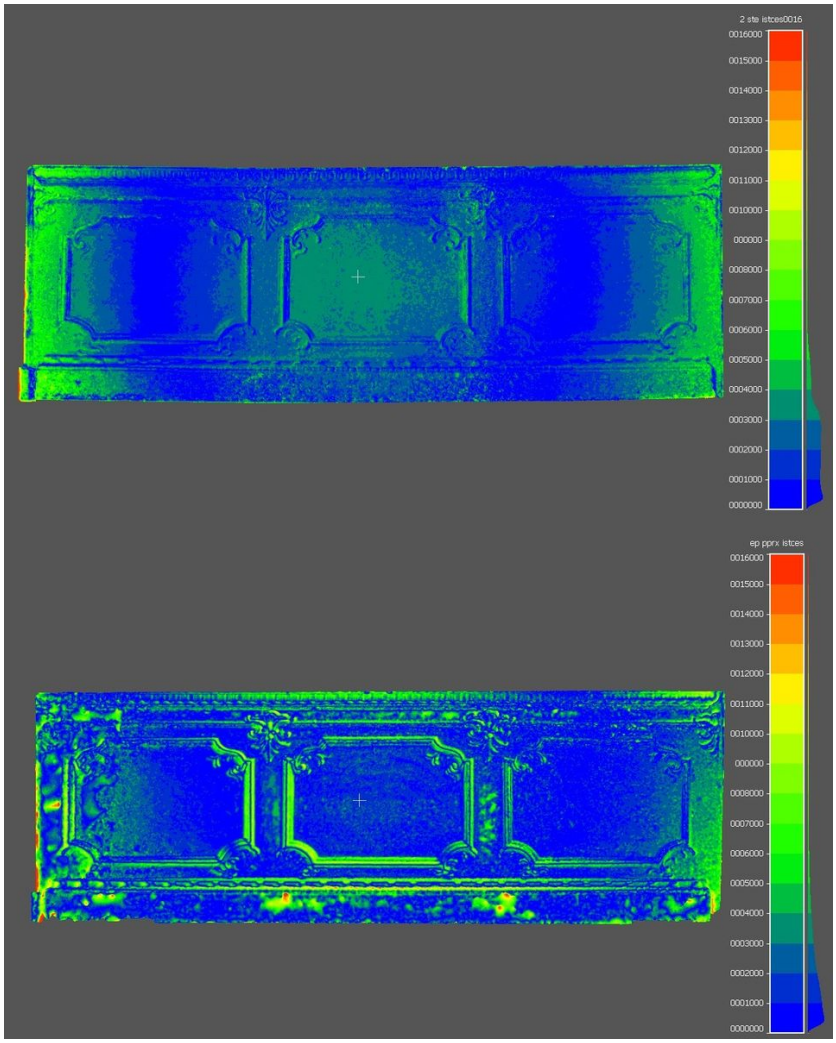

Figure 7

Wooden furniture part, geometric differences between visible and near-infrared spectra AMP models (top), geo-metric differences between visible spectrum models from two software (bottom; Hausdorff distances shown on a scale up to 8 mm, with 0.5 mm scalar field intervals)

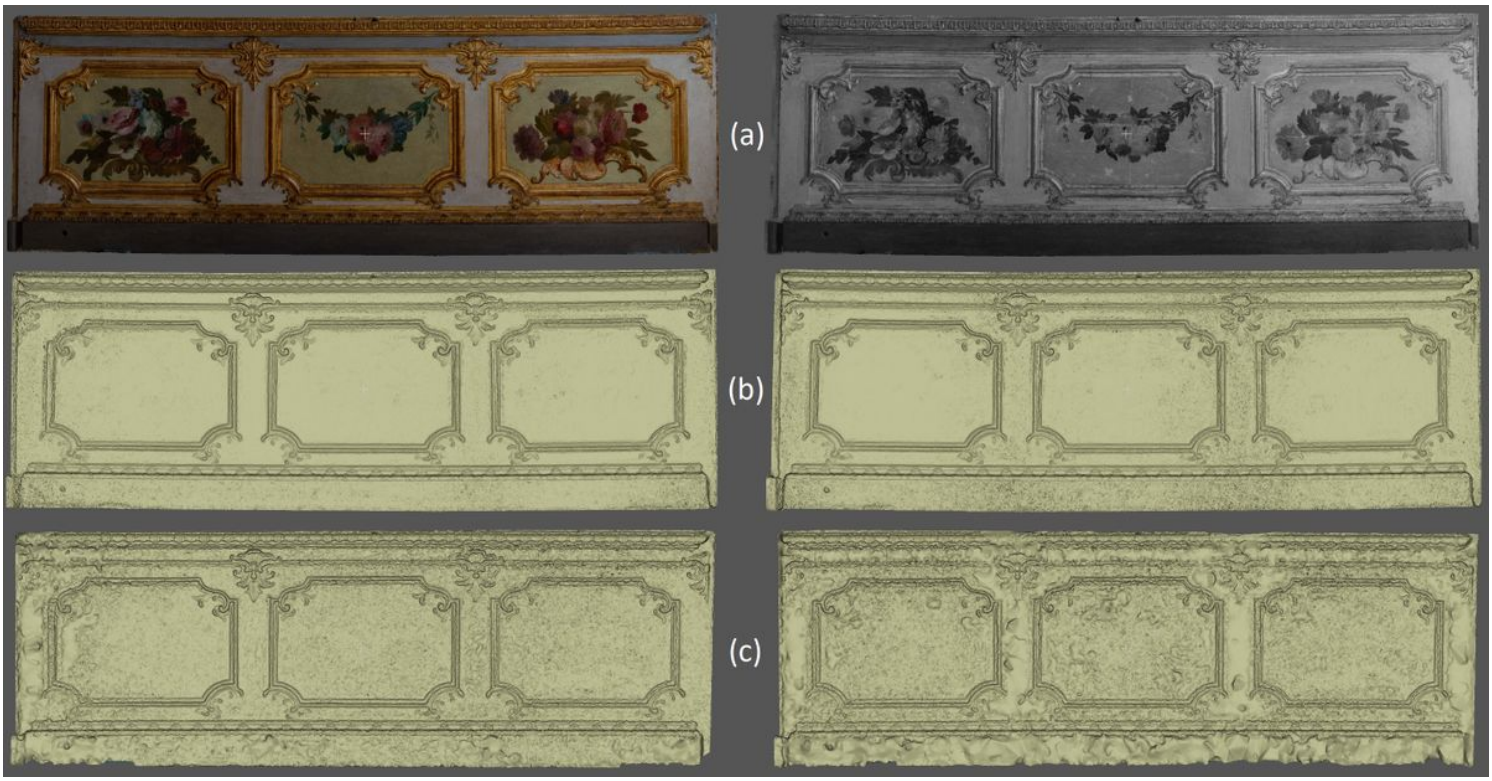

Figure 8

Wooden furniture part, dense image-based reconstruction results (left visible spectrum, right near-infrared spec-trum), a AMP textured mesh; b AMP untextured mesh; c FZA untextured mesh

Figure 9

Furniture part (detail), near-infrared texture orthophoto where cracks and re-touchments can be identified

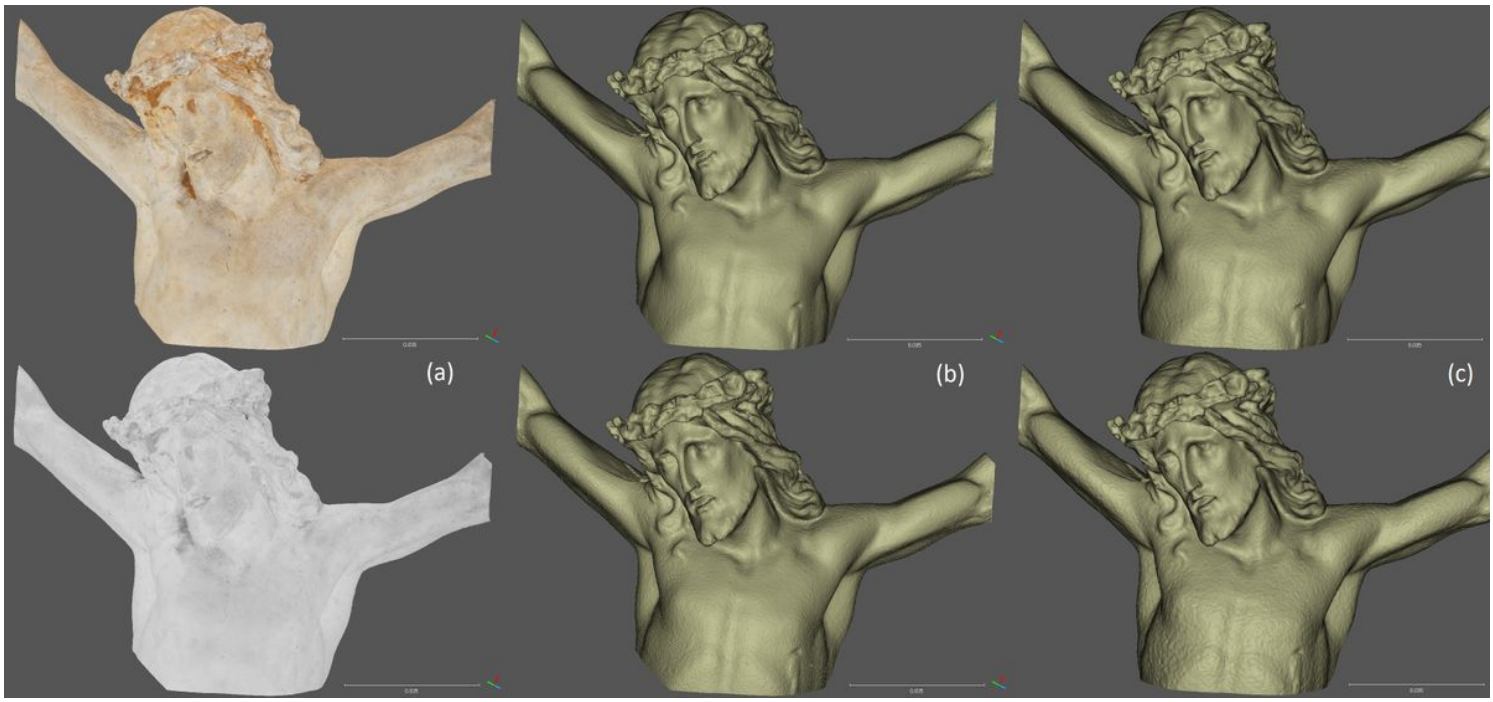

Figure 10

Sculpture of Christ, dense image-based reconstruction results (top visible spectrum, bottom near-infrared spec-trum), a AMP textured mesh; b AMP untextured mesh; c FZA untextured mesh

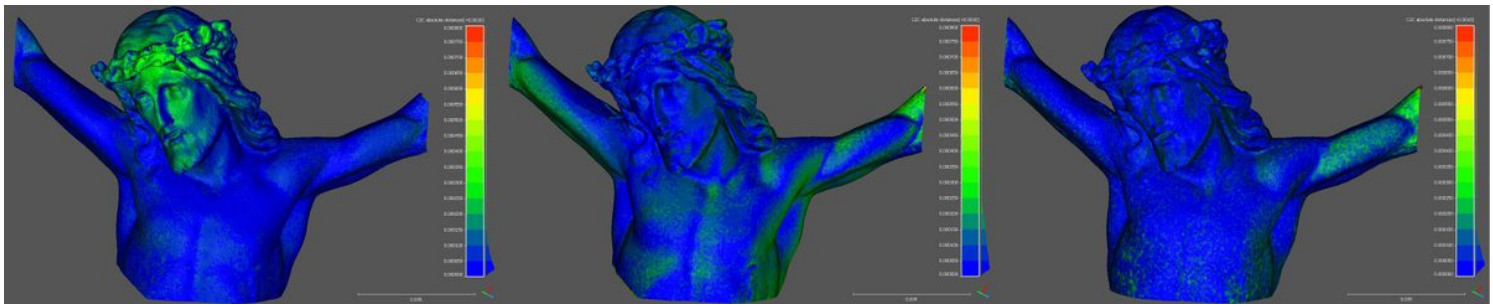

Figure 11

Sculpture of Christ, geometric differences between models, visible to near-infrared spectra for AMP (left); visible to near-infrared spectra for FZA (center); visible AMP to visible FZA (right); Hausdorff distances shown on a scale of max 0.8 mm, with 0.5 mm scalar field intervals)

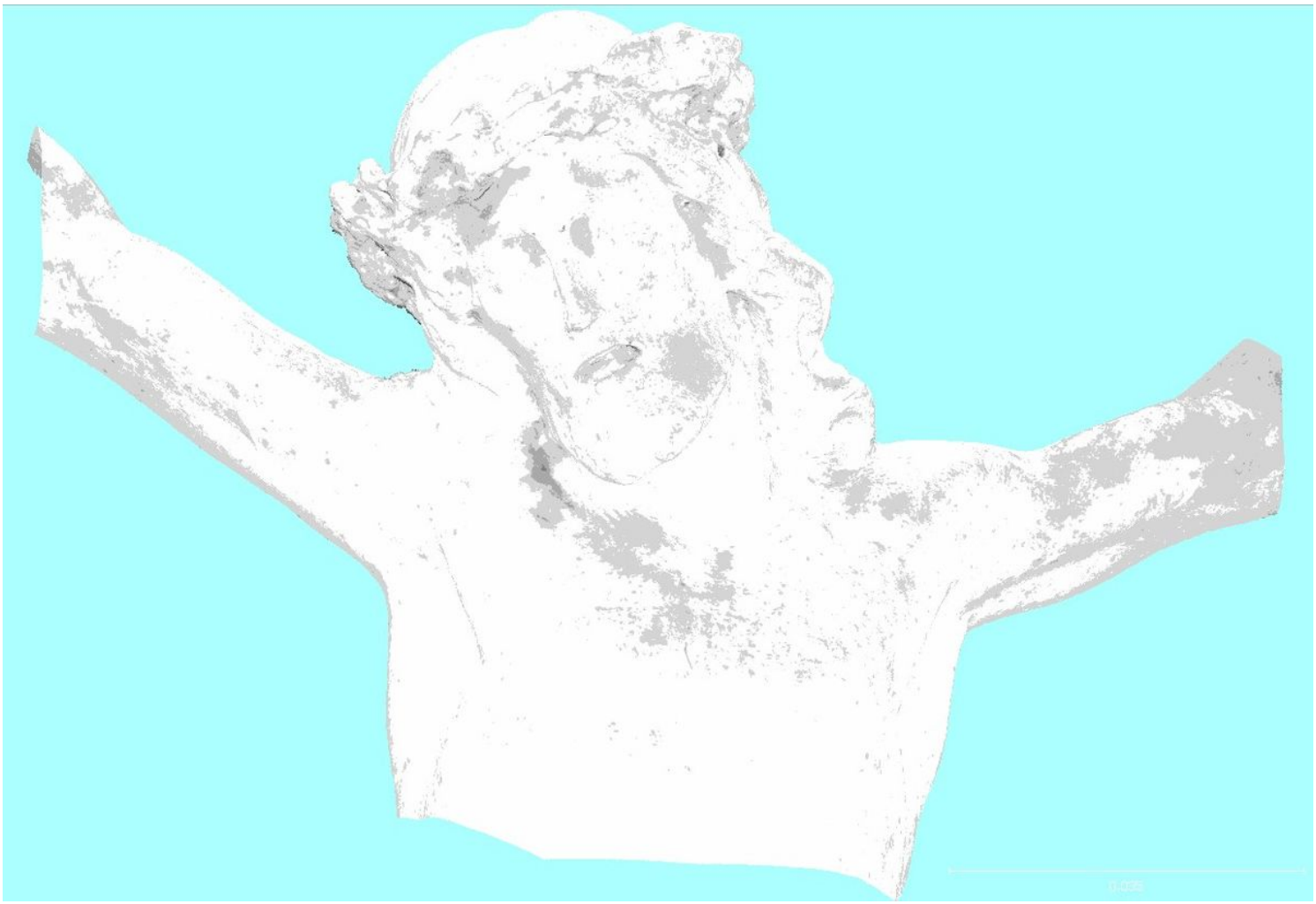

Figure 12

Sculpture of Christ, 6-group classification mapping of near-infrared intensities (right) from NIR AMP model